Transport of Sub-micron Aerosols in Bifurcations

Fong Yew Leong[a], Kenneth A. Smith[a,b], Chi-Hwa Wang[a,c]

[a] *Singapore-MIT Alliance,* [b] *Massachusetts Institute of Technology,* [c] *National University of Singapore*

Abstract – **The convective-diffusive transport of sub-micron aerosols in an oscillatory laminar flow within a 2-D single bifurcation is studied, using order-of-magnitude analysis and numerical simulation using a commercial software (FEMLAB®). Based on the similarity between momentum and mass transfer equations, various transient mass transport regimes are classified and scaled according to Strouhal and beta numbers. Results show that the mass transfer rate is highest at the carinal ridge and there is a phase-shift in diffusive transport time if the beta number is greater than one. It is also shown that diffusive mass transfer becomes independent of the oscillating outer flow if the Strouhal number is greater than one.**

Index Terms – **aerosol, convective-diffusive, lung, sub-micron**

I. Introduction

It is well-known that aerosol deposition in the lung is governed by three principal mechanisms: inertial impaction, sedimentation and Brownian diffusion. How and where particles deposit in the lung is affected by the size of the particles [1]:

- Particles larger than 15μm deposit solely by inertial impaction in extra-thoracic airways;
- Particles between 2-15μm deposit by inertial impaction in extra-thoracic airways and by gravitational sedimentation in thoracic airways;
- Particles smaller than 2μm deposit by gravitational sedimentation and Brownian diffusion in thoracic airways and alveolar airpaces.

Fong Yew Leong is with the Singapore-MIT Alliance, MEBCS Program, National University of Singapore, 4 Engineering Drive 3, Singapore 117576, Singapore

Kenneth A. Smith is with the Singapore-MIT Alliance and the Massachusetts Institute of Technology, 77 Massachusetts Ave Cambridge, MA 02139, USA

Chi-Hwa Wang is with the Singapore-MIT Alliance and the Department of Chemical and Biomolecular Engineering, National University of Singapore, 10 Kent Ridge Crescent, Singapore 119260, Singapore

There is a reasonably good understanding of how inertial impaction affects deposition in the lung even in oscillatory conditions, through computational CFD [2] and experimental work [3]. Gravitational sedimentation is a seemingly less interesting phenomenon, but even so, its effect on particles in oscillatory pipe flow has been investigated [4]. On the other hand, there have been relatively few investigations of transport of sub-micron aerosols in the lung, mainly due to the difficulty of aerosol generation and accurate predictions based on simulations [5].

Sub-micron aerosols are commonly inhaled from the ambient environment, workplace or therapeutic inhalers. Studies have shown that, due to their deep lung penetration capability, many types of sub-micron toxic aerosols are potentially more hazardous than their micron-sized counterparts [6, 7]. Or, in the case of therapeutic aerosols, smaller drug particles can also be more efficient tools for drug delivery [8].

As mentioned earlier, the transport of sub-micron aerosols in the lung is chiefly dominated by convective and diffusive mechanisms. In an analogous manner, the convective-diffusive equation has been used to solve the mass transfer problem for steady flow in straight pipes [9]. The significance of the entrance effects has also been recognized due to the relatively short tubes of each lung generation compared to the diameter [10]. Another analytical solution using a different approach [11] obtained an even better agreement with experimental studies [12].

As summarized in [13], there are several theoretical works on various isolated aspects of lung transport. However, to the best knowledge of this author, there is no reported work on the effects of oscillatory flow on the deposition of sub-micron particles for a generic bifurcated geometry. Nevertheless, a related topic does exist and it is the enhanced Taylor dispersion of gases in oscillatory pipe flows. Theoretical prediction of this phenomenon had been reported in [14], and

verified in a companion paper [15]. The effective dispersion was found to be affected strongly by the Womersley number [16], and the maximum dispersion can be produced by a resonance effect in a curved tube, when the oscillatory period equals the secondary flow time [17].

These theoretical predictions suggest by analogy that it may be possible to describe the deposition of submicron particles in oscillatory flow in a similar manner as for gases. The corresponding analyses will be given in the following chapters.

II. Theory

Unlike the case for gas transport in the lung, the diffusion transport of sub-micron aerosols is frequently much smaller than the convective transport (Peclet number >> 1). Large gradients of particle concentration exist near the walls, so the physics of the problem is essentially captured by the boundary layer theory. For the 2-D case, the relevant momentum, concentration and continuity boundary layer equations are set out below:

$$u\frac{\partial u}{\partial x}+v\frac{\partial u}{\partial x}=\nu\frac{\partial^2 u}{\partial y^2}-\frac{1}{\rho}\frac{dP}{dx} \quad (1)$$

$$\frac{\partial C}{\partial t}+u\frac{\partial C}{\partial x}+v\frac{\partial C}{\partial y}=D\frac{\partial^2 C}{\partial y^2} \quad (2)$$

$$\frac{\partial u}{\partial x}+\frac{\partial v}{\partial y}=0 \quad (3)$$

where u is the scalar fluid velocity in the x-direction, y is the scalar fluid velocity in the y-direction, ρ is fluid density, υ is kinematic viscosity, P is pressure, C is concentration of the particles, D is the diffusion coefficient of the particles and t is time.

For very large Schmidt numbers, the thickness of the concentration boundary layer is very thin compared to the fluid boundary layer, so the respective fluid velocity components can be effectively approximated by the 1st terms in the Taylor series expansions. A good description of this method can be found in [18].

Our transient transport problem however involves oscillatory boundary layers. Due to the fact that Womersley number in the lower airways is typically less than unity, *quasi-steady* condition can be assumed. If the momentum within the fluid boundary layer reacts instantly to the oscillating outer flow, the linearized velocity profile can be written as follows.

$$u=yB(x)\sin\omega t \quad (4)$$

$$v=-\frac{1}{2}y^2B'(x)\sin\omega t \quad (5)$$

where B(x) is the velocity derivative at the wall $B(x)=\left.\frac{\partial u}{\partial y}\right|_{y=0}$

This linearization of the near-wall steady-state velocity profile ensures that the continuity equation (3) is satisfied and is often referred to as the *Lévêque approximation.*

These equations (4, 5) are then substituted into concentration boundary layer equation (2) to reach:

$$\frac{\partial C}{\partial t}+\left[B(x)\frac{\partial C}{\partial x}-\frac{1}{2}yB'(x)\frac{\partial C}{\partial y}\right]y\sin\omega t=D\frac{\partial^2 C}{\partial y^2} \quad (6)$$

The physics of this complex concentration boundary layer problem has been neatly summarized in equation (6), highlighting transient, convective, and diffusive transport terms respectively. Unfortunately, it is exceedingly difficult to derive an analytical solution to this partial differential equation.

Hence, there is a case for numerical solution, and the method of choice is finite elements, using a commercial software known as FEMLAB®. The generic equations to be solved are the complete set of Navier-Stokes equation, convective-diffusive equation and the continuity equation.

$$\rho\left(\frac{\partial\bar{v}}{\partial t}+\bar{v}\cdot\nabla\bar{v}\right)=\rho g-\nabla P+\mu\nabla^2\bar{v} \quad (7)$$

$$\frac{\partial C}{\partial t}+\bar{v}\nabla C=\nabla D\nabla C \quad (8)$$

$$\nabla\cdot\bar{v}=0 \quad (9)$$

where $\bar{v}$ is the fluid velocity in vector form and μ is dynamic viscosity. The scalar shorthand for the velocities as used in the boundary layer equations no longer apply in the consideration of outer flow.

III. Dimensional analysis

The time dependent fluid motion is frequently characterized by the Womersley number and the Strouhal number [19].

$$\alpha=L\sqrt{\frac{\omega}{\nu}} \quad (10)$$

$$Sr=\frac{\alpha^2}{\mathrm{Re}}=\frac{\omega L}{U} \quad (11)$$

where α is the Womersley number, L is characteristic length of the system, ω is the frequency of oscillation, Sr is the Strouhal number, and U is the fluid velocity.

If the viscosity variable in equation (10) is replaced by the Brownian diffusion coefficient of the aerosol (D), we have instead the beta number.

$$\beta = L\sqrt{\frac{\omega}{D}} \tag{12}$$

$$Pe = \frac{\beta^2}{Sr} = \frac{UL}{D} \tag{13}$$

The Strouhal number (11), the beta number (12), and the Peclet number (13) will form the basis for the characterization of our mass transfer regimes. Using order-of-magnitude arguments, the dominance of the transport regimes has to depend mainly on the Strouhal or beta numbers being greater or less than one. Hence, we can sketch the following map showing the dominance of each term in the convective-diffusive equation (Fig. 1).

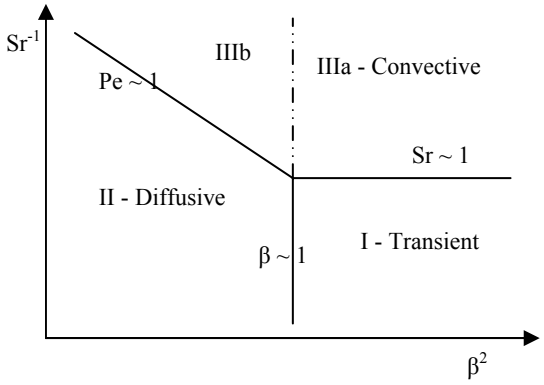

Fig. 1. Mass Transfer Regimes

Fig. 1 resembles the momentum transport flow regime map presented in [19]. Their experimental work identified observable differences between high and low Womersley numbers, even within the same convective-dominated regime. This is the reason for the separation of the convection-dominated regime into Zone IIIa and IIIb.

It is extremely unlikely that the Peclet or Schmidt numbers for diffusion of sub-micron particles to be less than unity, so Zone II for diffusion-dominated transport will not be considered in this study. Diffusive transport is almost always convective-dominated (Zone IIIa and IIIb) or transient-dominated (Zone I). These cases will be examined subsequently.

IV. Simulations

Numerical simulations using finite elements are conducted on FEMLAB® v3.0. Dimensions of the 2-D bifurcation model used correspond to 13th to 14th generation of the Weibel's morphometric lung model-A [20], which is representative of the lower airways, but it should be noted that this selection is arbitrary and does not indicate any form of specific constraint in the simulation.

All the dynamic variables used in subsequent simulations are effectively non-dimensionalized. The only variable left to be scaled is the local Reynolds numbers. This scaling approach is valid due to the monotonically increasing total cross-sectional area with increasing lung generations (the well-known 'trumpet' model).

More than 10,000 finite elements are used in each case, with the exact figure depending on the demands of the specific problem. The mesh concentration near the boundaries is at least twice the overall average, due to higher gradients of variables at boundary layers.

The dimensional parameters of the meshed bifurcation model are shown in Fig. 2. The bifurcation angle is set at 90º.

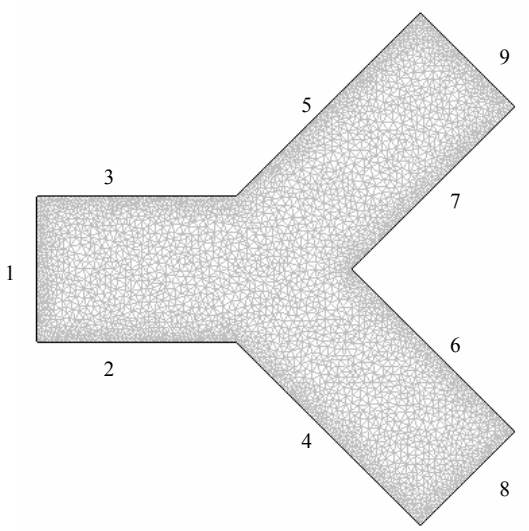

Edge	Length (mm)
1	0.70
2-3	0.95
4-5	1.24
6-7	1.10
8-9	0.64

Fig. 2. Meshed Single 2-D Bifurcation Model

Other parameters used in the simulations are listed below:

- **Initial Conditions**
  - $U_i = 0$
  - $C_i = C_0$
- **Inlet Conditions (Edge 1)**
  - $U_{in} = U_0 * \sin(\omega t)$
  - $C_{in} = C_0$
- **Wall Conditions (Edges 2-7)**
  - No-slip condition
  - No concentration condition, $C_{wall} = 0$
- **Outlet Conditions (Edges 8-9)**
  - Null Pressure condition
  - Convective flux only

where U is the fluid velocity, C is the aerosol concentration, ω is the frequency parameter, and t is time.

The inlet velocity profile is always uniform, and it oscillates sinusoidally with time. The no-concentration condition imposed at the boundaries is valid based on the rapid adherence of the sub-micron particles to the moist walls [5].

For the numerical solution of the problem, the multi-physics function of FEMLAB® is invoked, which couples the computation for all the equations (7)-(9). The system solver used is UMFPACK, which is an efficient non-iterative direct solver used for unsymmetric non-linear systems. The relative and absolute tolerance limits are set at 0.001 and 0.0001 respectively.

A. Convection-dominated Transport (Zone IIIa)

For Zone IIIa, the peak Reynolds number is taken to be 0.5. This is one order of magnitude less than the characteristic Reynolds number, which increases computational efficacy but does not affect the overall results significantly. Time is normalized against the half-period of oscillation, which is simply 1s. The inlet aerosol concentration C_0 is simply taken as normalized unity. The inlet velocity profile is uniform and the peak inlet velocity U_0 is set at 0.012m/s. The Brownian diffusion coefficient of the 0.1 micron aerosols is $6.8 \times 10^{-10} m^2/s$.

These parameter values are used to calculate the important dimensionless groups that have been identified earlier. These values are tabulated in Table 1 as shown.

Dimensionless numbers (Zone IIIa)		
Womersley, alpha	0.15	< 1
Beta	23.8	> 1
Strouhal	0.09	< 1

Table 1. Important Dimensionless Groups (Zone IIIa)

Each half-cycle (1s) of the periodic velocity wave is simulated sequentially, with the final results of the previous run being used as the initial conditions for the new run. This is to allow the inlet and outlet boundary conditions to be switched at the start of each new half-cycle.

The concentration fields shown in Fig. 3 are taken at the end of the first two half-cycles of inhalation (time 1.0) and exhalation (time 2.0) respectively.

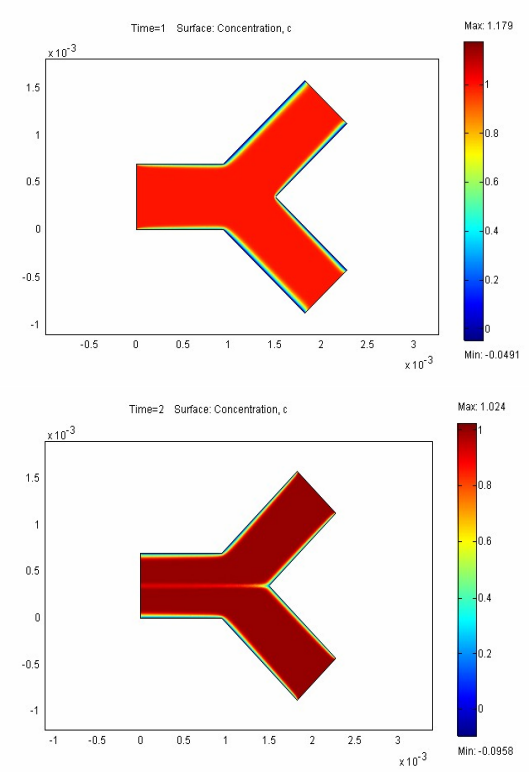

Fig. 3. Concentration Profiles for Convective Transport (Top: Inhalation half-cycle; Bottom: Exhalation half-cycle)

There are a couple of observations. The very thin concentration boundary layer is due to the large Peclet number used. The concentration wake formed during expiration half-cycle (see Fig. 3. Bottom) is due to the convective transport of the low concentration fluid from the boundary layer to the outer flow.

In fact, these observations reflect the dominance of the convective term in equation (6). The secondary dominance of either the transient or diffusive term will affect the other aspects of the transport, and that is related to the beta number.

Other than the concentration profiles, the simulation also indicates the intuitive result that the extremely thin concentration boundary layer at the carinal ridge (leading edge) leads to the highest rates of diffusive wall mass flux. The arc A-B-C as shown in Fig. 4 is used in the plots of the normal diffusive mass flux as shown in Fig. 5. In this example, the various curves reflect the instantaneous fluxes in time, in three intervals from 2 to 3s.

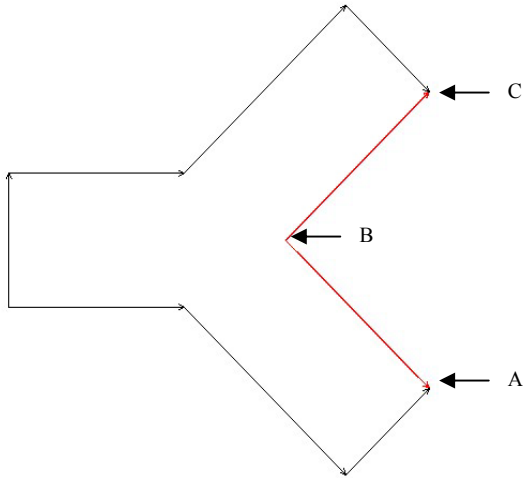

Fig. 4. Schematic Diagram of Model
(Arc A-B-C is used in Fig. 5)

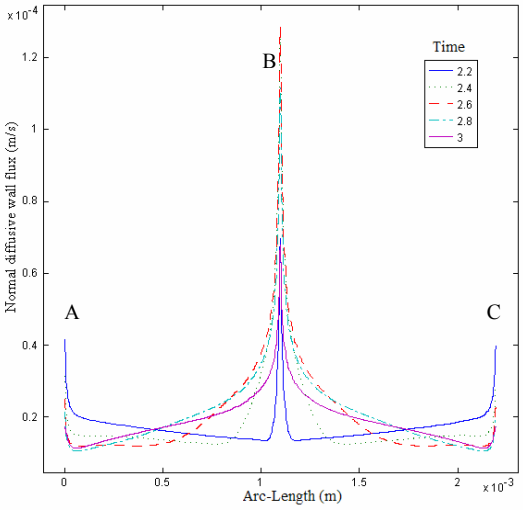

Fig. 5. Plot of Normal Diffusive Wall Mass Flux against Arc-length (Legend indicates dimensionless time of the curves)

When the normal diffusive wall mass fluxes (e.g. Fig. 5) are integrated over the entire surface wall boundaries (Edges 2-7), they yield the overall deposition rate of the sub-micron particles within the control volume. This can be normalized against the diffusion coefficient to yield a dimensionless number, which can be correlated to the Sherwood number (Sh) in the following manner:

$$Sh = \frac{k_c L}{D} \sim \frac{\oint (N_{diff}) ds}{D} \qquad (14)$$

where k_c is the mass transfer coefficient, L is the characteristic length, D is the diffusion coefficient, N_{diff} is the normal diffusive mass flux, and s is the local wall length-scale.

The above correlation is based on the zero concentration boundary condition and the purely diffusive contribution to the normal mass flux.

Since convective transport is the dominant mode of mass transfer, there is a strong functional dependence of the average Sherwood number on the fluid velocity at the inlet, which is expressed as Reynolds number (Re). Both parameters are plotted as a function of the dimensionless time for seven half-cycles in Fig. 6.

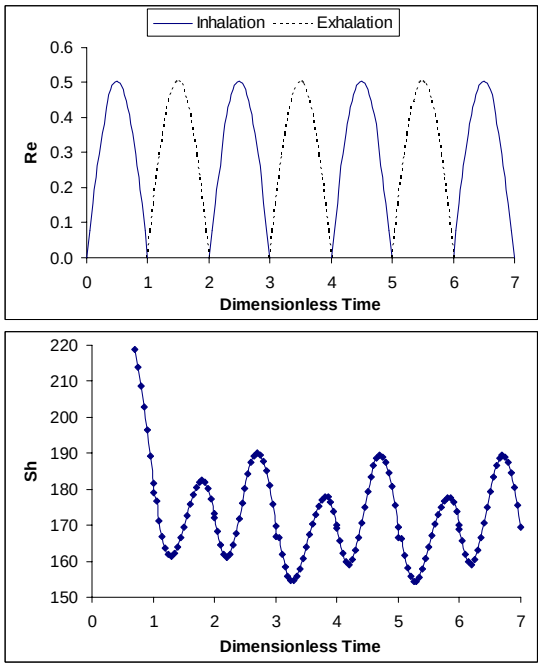

Fig. 6. Time Evolution of Reynolds and Sherwood numbers at $\beta > 1$, $Sr < 1$ (Zone IIIa)

The average Sherwood number (Fig. 6: Bottom) starts off from a very high value (not shown), due to the initial domain concentration condition, and declines with time, until the dimensionless time is ~1. Then it oscillates periodically with the fluid momentum cycles (Fig. 6: Top), due to the convective term in equation (6). This fluctuation correlates directly to the oscillations of the fluid velocity at the inlet, since fluid momentum is quasi-steady (Table 1). The significance of the convective term can also be deduced from the relatively large average Sherwood number.

It is also observed that inhalation phase produces more transport than the exhalation phase, which suggests that the mass transfer at the leading edge (Vertex B in Fig. 4 and 5) is enhanced significantly. In addition, there is a substantial phase lag between the mass transfer cycles and the imposed fluid oscillation cycles. This indicates that there is a difference in time scales between the convective fluxes and the diffusive fluxes, which is due to the beta number being greater than unity, so concentration is not quasi-steady.

B. Convection-dominated Transport (Zone IIIb)

As shown in Fig. 1, there is another region of convective-dominated transport, in which both fluid and mass transfer are quasi-steady in relation to the oscillating outer flow. This region is characterized by a beta number lower than unity and is referred to as Zone IIIb, in contrast to the Zone IIIa as studied earlier.

Another simulation run is conducted at a beta number lower than one. This is achieved by increasing the diffusion coefficient by two orders of magnitude to 6.8 x $10^{-8}m^2/s$, representing smaller particles ~10nm. The half-cycle time is also increased from 1s to 10s, representing very slow breathing. The effects of these changes on the important dimensionless parameters are tabulated in Table 2.

Dimensionless numbers (Zone IIIb)		
Womersley, alpha	0.05	< 1
Beta	0.75	< 1
Strouhal	0.009	< 1

Table 2. Important Dimensionless Groups (Zone IIIb)

Comparing Tables 1 and 2, it should be recognized that the new beta number is now less than unity, whereas the status of other dimensionless groups remain unchanged.

As before, through the integration of the normal diffusive wall mass fluxes and the input velocity, we obtain the Sherwood and Reynolds numbers respectively. Both parameters are plotted as a function of the dimensionless time for four half-cycles in Fig. 7.

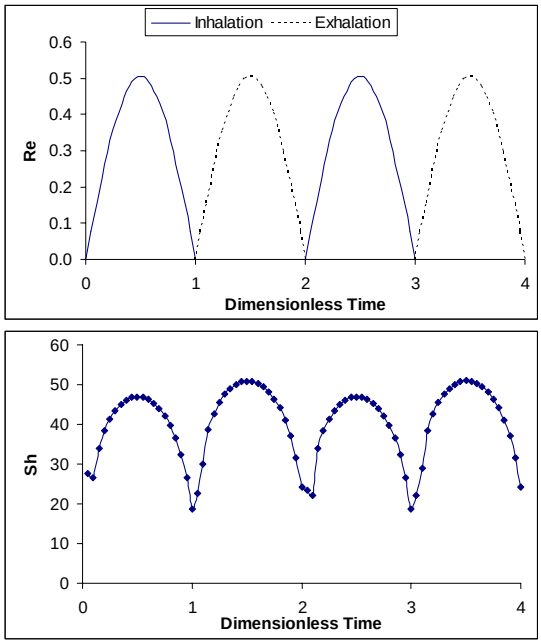

Fig. 7. Time Evolution of Reynolds and Sherwood numbers at $\beta < 1$, $Sr < 1$ (Zone IIIb)

The average Sherwood number (Fig. 7: Bottom) also starts off from a very high value (not shown), and declines very rapidly to ~ 30, and later oscillates periodically with time. A comparison between Fig. 6 and 7 shows that the phase lag noted earlier has diminished. The normal diffusion wall mass flux is now quasi-steady with respect to the oscillatory outer flow. This verifies our predictions of the differences between Zone IIIa and Zone IIIb (Fig. 1) and this highlights the importance of the beta number to the oscillatory flow diffusion problem in bifurcations.

It is also observed that the difference in transport magnitudes between inhalation and exhalation phases is no longer significant. In addition, it should be noted that the overall magnitude of Sherwood number is much lower for

the Zone IIIb case than for Zone IIIa case earlier. Steady state mass transfer theory suggests a power law dependence of the Sherwood number (Sh) on the Schmidt number (Sc).

$$\frac{Sh_1}{Sh_2} = \left(\frac{Sc_1}{Sc_2}\right)^a \tag{15}$$

where a is the power law exponent

From Fig. 6, the mean average Sherwood number is ~ 170 for Schmidt number of 12,353, whereas from Fig. 7, the mean average Sherwood number is ~ 35 for Schmidt number of 124. The global average power law exponent (a) is thus estimated to be 0.343, which is close to the familiar scale of 0.333 (one-third) for concentration boundary layers for steady flows. Examination of other combinations of the same manipulated variables also yields similar results.

C. Transient-dominated Transport (Zone I)

Simulation work for Zone I has been conducted with essentially the same parameters and conditions as for the convection-dominated transport (0.1 micron particles, 1s half-cycle), except that the peak Reynolds number is reduced by two-orders of magnitude to 0.005 (representing very deep airways). This change is reflected in Table 3.

Dimensionless numbers (Zone I)		
Womersley, alpha	0.15	< 1
Beta	23.8	> 1
Strouhal	9.2	> 1

Table 3. Important Dimensionless Groups (Zone I)

Comparing Tables 1 and 3, we see that the Strouhal number is now greater than unity, whereas the status of other dimensionless groups remain unchanged. This places us in the transient-dominated regime (Fig. 1).

The simulation run for this case is conducted for three complete cycles. The concentration fields taken at the end of half-cycles (time 3.0 and 4.0 for inhalation and exhalation phases respectively) are shown in Fig. 8.

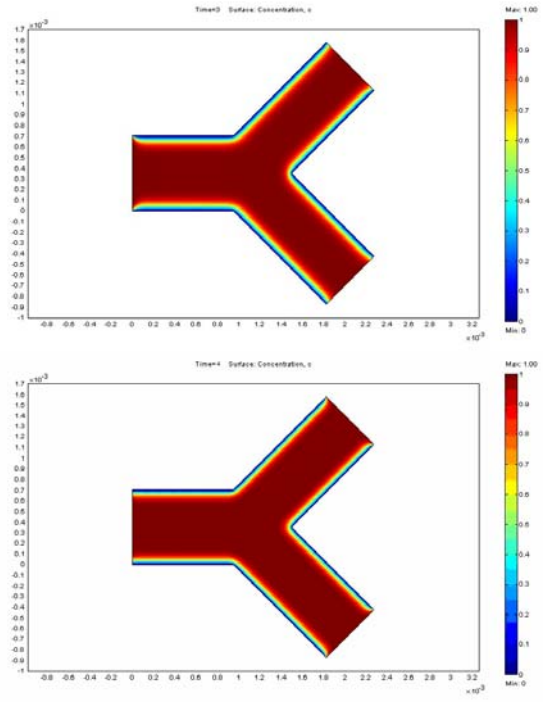

Fig. 8. Concentration Profiles for Transient Transport
(Top: Inhalation half-cycle; Bottom: Exhalation half-cycle)

Comparing Fig. 3 and 8, some differences in the concentration field can be observed. For the inhalation half-cycle, the concentration boundary layer at the leading edge (carinal ridge) is extremely thin for convection-dominated transport (Fig. 3: Top), whereas this leading edge phenomenon is not observable for transient-dominated transport (Fig. 8: Top). In fact, the wall mass diffusive flux is now independent of the distance from the leading edge.

For the exhalation half-cycle, a concentration wake was observed earlier for convection-dominated transport (Fig. 3: Bottom), but this is evidently absent in the case of transient-dominated transport (Fig. 8: Bottom). This is due to the fact that the diffusion is of the same order as the convection, so the low concentration fluid attains the concentration of the surrounding fluid as soon as it leaves the trailing edge region (carinal ridge).

Following the same procedure as for the convection-dominated case, the normal diffusive wall mass flux is integrated to yield the Sherwood number (Sh) and this is plotted as a function of time, alongside the Reynolds number (Re) for seven half-cycles (Fig. 9).

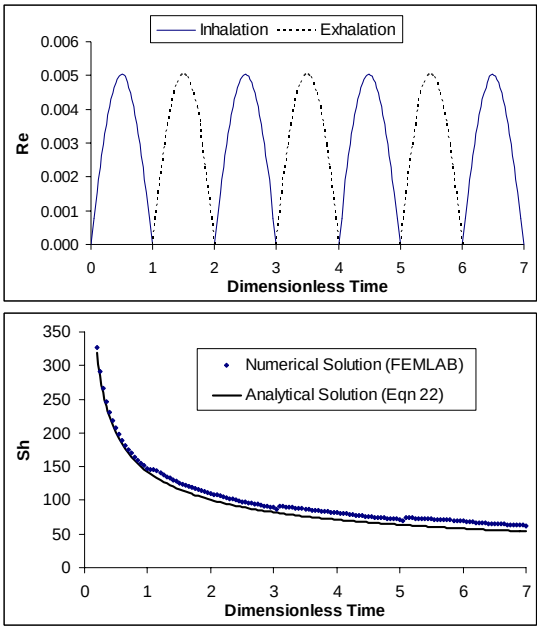

Fig. 9. Time Evolution of Reynolds and Sherwood numbers at $\beta > 1$, $Sr > 1$ (Zone I)

From Fig. 9, it is evident that the mass transfer rate is now independent of the oscillating outer flow, in sharp contrast with the case of convection-dominated transport (Compare with Fig. 6 and 7).

In addition, the diffusion rate is declining constantly and steadily with time, from the initial concentration condition we have set. This can be explained by the observation that, if we eliminate the convective terms from equation (6), it becomes simply

$$\frac{\partial C}{\partial t} = D\frac{\partial^2 C}{\partial y^2} \tag{15}$$

This is the standard form for the well-known 1-D unsteady 'heat-conduction' equation. In fact, by introducing a similarity variable (η), an analytical solution to equation (15) is available.

$$\frac{C}{C_0} = 1 - erf(\eta) \tag{16}$$

where

$$\eta = \frac{y}{2\sqrt{Dt}} \tag{17}$$

$$erf(\eta) = \frac{2}{\sqrt{\pi}}\int_0^{\eta} e^{-\eta^2} d\eta \approx \frac{2}{\sqrt{\pi}}\left(\eta - \frac{\eta^3}{113} + \frac{\eta^5}{215} - \ldots\right) \tag{18}$$

Using the similarity variable (17), the normal mass flux at the walls can be defined as

$$N_y\Big|_{y=0} = -D\frac{\partial C}{\partial y}\Big|_{y=0} = -\frac{C_0}{2}\sqrt{\frac{D}{t}}\left(\frac{d\hat{C}}{d\eta}\Big|_{\eta=0}\right) \tag{19}$$

where $\hat{C}$ is the normalized concentration.

The derivative of the expansion of the error function (18) resolved at the wall is simply

$$\frac{d\hat{C}}{d\eta}\Big|_{\eta=0} = -\frac{2}{\sqrt{\pi}} \tag{20}$$

Substitution of (20) in (19) yields

$$N_y\Big|_{y=0} = \sqrt{\frac{D}{\pi t}} \tag{21}$$

Equation (21) is then used in the definition of the average Sherwood number (14). Due to the independence of the normal mass flux on the wall length-scale, we can write

$$Sh = \frac{\oint\left(N_y\Big|_{y=0}\right)ds}{D} = \frac{S}{\sqrt{D\pi t}} \tag{22}$$

where S is the global wall length, as defined in our model by the sum of lengths of edges 2 to 7 (refer to Fig. 2), which is 6.58mm, and D the diffusion coefficient is $6.8 \times 10^{-10} m^2/s$ as defined earlier.

Equation (22) is then plotted against time and compared with the numerical solution from FEMLAB®, as shown in Fig. 9. The excellent fit between the analytical and numerical solutions not only demonstrates the analytical simplifications in Zone I, but also validates the conclusions reached earlier based on numerical simulations.

Qualitatively, the rate at which particles are deposited at the walls is faster than the rate of material influx into the control volume through convection. This leads to particle depletion in the boundary layer and the decline in concentration gradients results in the decrease in diffusion rate.

V. Conclusion

Through effective non-dimensionalization of the problem, we can extend the qualitative solutions to any other generations of the Weibel's lung [20], simply by scaling to the appropriate local Reynolds number. Hence, based on the approach outlined in this paper and the simulation results, there is no loss of generality and we may obtain an overall description of the transport phenomena of sub-micron aerosols in the lung.

This apparent extensibility carries a limitation, however. The inherent assumption of scaling is that the solutions, carried out under laminar flow conditions, are entirely independent of Reynolds numbers. This does not hold under certain conditions, notably in the trachea and uppermost airways, where turbulence and flow separation phenomena are prevalent. These exceptions will form the basis of future work.

REFERENCES

[1] J. Heyder, J. Gebhart, G. Rudolf, C.F. Schiller, W. Stahlhofen. *Deposition of particles in the human respiratory tract in the size range 0.005-15 μm*. J. Aerosol Sci. 17(5), 811-825, 1986.

[2] Z. Zhang, C. Kleinstreuer, C.S. Kim. *Cyclic micron-size particle inhalation and deposition in a triple bifurcation lung airway model*. J. Aerosol Sci. 33, 257-281, 2002.

[3] C.S. Kim, and D.M. Fisher. *Deposition characteristics of aerosol particles in sequentially bifurcating airway models.* Aerosol Sci. Tech. 31, 198-220, 1999.

[4] M. Kojic, and A. Tsuda. *A simple model for gravitational deposition of non-diffusing particles in oscillatory laminar pipe flow and its application to small airways*. J. Aerosol Sci. 35, 245-261, 2004.

[5] Z. Zhang, and C. Kleinstreuer. *Airflow structures and nano-particle deposition in a human upper airway model.* J. Comp. Phys. 198, 178-210, 2004.

[6] M.W. Frampton, *Systemic and cardiovascular effects of airway injury and inflammation: ultrafine particle exposure in humans*, Environ. Health Perspectives 109, 529-532, 2001.

[7] K. Donaldson, X.Y. Li, W. Macnee. *Ultrafine (nanometer) particle-mediated lung injury.* J. Aerosol Sci. 29, 553-560, 1998.

[8] D.A. Edwards. *Delivery of biological agents by aerosols.* AIChE J. 48(1), 2-6, 2002.

[9] D.B. Ingham. *Diffusion of aerosols from a stream flowing through a p cylindrical tube.* J. Aerosol Sci. 6, 125-132, 1975.

[10] D.B. Ingham *Diffusion of aerosols from a stream flowing through a short cylindrical pipe.* J. Aerosol Sci. 15(5), 637-641, 1984.

[11] T. Martonen, Z. Zhang, Y. Yang. *Particle diffusion with entrance effects in a smooth-walled cylinder.* J. Aerosol Sci. 27(1), 139-150, 1996.

[12] B.S. Cohen and B. Asgharian. *Deposition of ultrafine particles in the upper airways: an empirical analysis*. J. Aerosol Sci. 21, 789-795, 1990.

[13] H. Shi, C. Kleinstrueer, Z. Zhang, C.S. Kim. *Nanoparticle transport and deposition in bifurcating tubes with different inlet conditions.* Phys. Fluids 16(7), 2199-2213, 2004.

[14] E.J. Watson. *Diffusion in oscillatory pipe flow*. J. Fluid Mech. 133, 233-244, 1983.

[15] C.H. Joshi, R.D. Kamm, J.M. Drazen, A.S. Slutsky. *An experimental study of gas exchange in laminar oscillatory flow.* J. Fluid Mech 133, 245-254, 1983.

[16] D.M. Eckmann, and J.B. Grotberg. *Oscillatory flow and mass transport in a curved tube. J. Fluid Mech.* 188, 509-527, 1988.

[17] T.J. Pedley and R.D. Kamm. *The effect of secondary motion on axial transport in oscillatory tube flow.* J. Fluid Mech. 193, 347-367, 1988.

[18] J.S. Newman. Electrochemical Systems, 2nd ed. Prentice Hall Int. Series. 1991.

[19] D.L. Jan, A.H. Shapiro, R.D. Kamm. *Some features of oscillatory flow in a model bifurcation.* J. Appl. Physio. 67(1), 147-159, 1989.

[20] E.R. Weibel. Morphometry of the human lung. Academic Press, New York. 1963.